pharmaceutics

MDPI

Article

The Role of Hidden Conformers in Determination of Conformational Preferences of Mefenamic Acid by NOESY Spectroscopy

Konstantin V. Belov [1], Luís A. E. Batista de Carvalho [2], Alexey A. Dyshin [1], Sergey V. Efimov [3] and Ilya A. Khodov [1,*]

[1] Krestov Institute of Solution Chemistry, Russian Academy of Sciences, Ivanovo 153045, Russia
[2] Molecular Physical-Chemistry R&D Unit, Department of Chemistry, University of Coimbra, 3004-535 Coimbra, Portugal
[3] Institute of Physics, Kazan Federal University, Kazan 420008, Russia
* Correspondence: iakh@isc-ras.ru

Abstract: Mefenamic acid has been used as a non-steroidal anti-inflammatory drug for a long time. However, its practical use is quite limited due to a number of side effects on the intestinal organs. Conformational polymorphism provides mefenamic acid with unique properties regarding possible modifications obtained during the micronization process, which can improve pharmacokinetics and minimize side effects. Micronization can be performed by decompression of supercritical fluids; methods such as rapid expansion of the supercritical solution have proven their efficiency. However, this group of methods is poorly applicable for compounds with low solubility, and the modification of the method using a pharmaceutically suitable co-solvent may be useful. In our case, addition of only 2 mol % dimethyl sulfoxide increased the solubility remarkably. Information on the conformational state may be critically important for carrying out micronization. In this work, structural analysis and estimate of conformational preferences of mefenamic acid in dimethyl sulfoxide − d_6 (at 25 °C and 0.1 MPa) and in a mixed solvent supercritical carbon dioxide + dimethyl sulfoxide-d_6 (45 °C, 9 MPa) were performed based on nuclear Overhauser effect spectroscopy. Results show changes in the conformation fractions depending on the medium used. The importance of allowing for hidden conformers in estimating the conformational state was demonstrated in the analysis. Obtained results may be useful for improving micronization parameters.

Keywords: supercritical fluid; fenamates; spatial structure; high-pressure NMR

Citation: Belov, K.V.; Batista de Carvalho, L.A.E.; Dyshin, A.A.; Efimov, S.V.; Khodov, I.A. The Role of Hidden Conformers in Determination of Conformational Preferences of Mefenamic Acid by NOESY Spectroscopy. *Pharmaceutics* **2022**, *14*, 2276. https://doi.org/10.3390/pharmaceutics14112276

Academic Editors: Bogdan Stefan Vasile and Ionela Andreea Neacsu

Received: 4 October 2022
Accepted: 21 October 2022
Published: 24 October 2022

1. Introduction

Development and bringing to market of new pharmaceuticals is an arduous, time-consuming, and expensive process [1]. Invention and promoting each new drug can cost more than one billion dollars [2]. Thus, repurposing already existing drugs attracts increasingly more interest [3]. Implementation of this approach costs several million dollars, and the probability of approving a reprofiled drug by controlling agencies, such as the United States Food and Drug Administration, is higher [2,3]. Therefore, studies aimed at seeking new ways of drug repurposing among compounds already in use or those which have been withdrawn become urgent [4–6]. Fenamates give an example of such compounds; until 2012, they were used as non-steroidal anti-inflammatory drugs for pain relief. Due to a number of side effects, their use was ceased in some countries [7–9]. Recently, anti-cancer activity of fenamates was revealed [10–12].

Drug repurposing for returning a drug back to the pharmaceutical market requires a dramatic decrease in its side effects. This can be achieved by increasing its bioavailability with the aid of micronization. Micronized particles of the active pharmaceutical ingredient (API) possess a highly improved dissolution rate [13–15], which makes it possible to decrease the therapeutic dose and diminish side effects. An approach based on carbon dioxide supercritical fluid techniques is one of the highly efficient API micronization methods [16]. Depending on the solubility of the compound, different fluid-based micronization techniques are used. For materials well soluble in $scCO_2$ ($\gamma > \times10^{-3}$ M), methods based on the principal functions of CO_2 supercritical fluid expansion (RESS, PGSS, RESOLV, etc.) [17–19] are employed; for poorly soluble drugs ($\gamma < \times10^{-3}$ M), methods based on dilution of liquids by supercritical fluids (SAS, GAS, ASES, etc.) [20,21] can be used. All the mentioned methods have their advantages and drawbacks. For example, methods relying on expansion of $scCO_2$ produce smaller particles as compared with the dilution of liquids by the supercritical fluid. Fenamates have low solubility in $scCO_2$, so the dilution-based approaches are used most often for them [22–24]. Adaptation of the $scCO_2$ expansion methods for low-soluble compounds is an enticing idea. For instance, it was implemented in the Depressurization of an Expanded Liquid Organic Solution (DELOS) method [25]. Use of DMSO was proposed in [26] as a means of increasing the solubility of fenamates in $scCO_2$; therefore, we suppose the fluid expansion method of micronization can be applied to fenamates with the aid of this co-solvent. Controlling the polymorphic composition of pharmaceutical compounds is also important for obtaining micronized forms. This is especially so for mefenamic acid in $scCO_2$, since an unambiguous correlation was shown between polymorphism and conformational state in solution [27], and recrystallization of mefenamic acid under pressure was observed [28]. Hence, this compound is a perfect object to investigate.

The study of poorly soluble drug-like compounds at supercritical state parameters is a serious problem, and the selection of experimental methods for establishing the spatial structure of poorly soluble compounds is an urgent task. In this work, we aimed to estimate preferred conformers existing in solution upon addition of DMSO-d_6 to $scCO_2$. Addition of DMSO as the co-solvent is proposed as a novel, promising modification of high-pressure NMR technique. Obtained results may be of use in studies of other fenamates and are important for obtaining micronized forms with simultaneous control of polymorphism.

2. Materials and Methods

1D (^{1}H, ^{13}C) и 2D (^{1}H-^{13}C HSQC, ^{1}H-^{13}C HMBC, ^{1}H-^{1}H TOCSY, ^{1}H-^{1}H NOESY) spectra were recorded on a Bruker Avance III 500 MHz spectrometer. The sample temperature was maintained at 25 °C (for solution) and 45 °C (for fluid) with an accuracy of ± 0.10 °C. The ^{1}H and ^{13}C resonance frequencies were 500.17 and 125.79 MHz, respectively. The mefenamic acid (MFA, Sigma Aldrich Rus, Moscow, Russia, >99.99 % (*wt*/*wt*)) was used without additional purification. Deuterated dimethyl sulfoxide (DMSO-d_6, Sigma-Aldrich, Moscow, Russia 99.9 atom percent D) and carbon dioxide (GOST 8050-85, Linde Group, Moscow, Russia CO_2—99.995%, H_2O—<0.001%) were used as solvents for NMR studies. The MFA was dissolved in DMSO-d_6 to prepare solutions with saturated concentrations as high as 283 mg/mL. The NMR experiments at supercritical parameters of the state of CO_2 were carried out using equipment of the unique scientific facility, "Fluid-Spectr" (https://ckp-rf.ru/usu/503933/ accessed on 4 October 2022), of G.A. Krestov institute of solution chemistry of RAS for maintaining pressure in real-time.

Carbon dioxide from a gas cylinder (position 1 in Figure 1) was used for the addition of high-pressure NMR cell (patent RU201791U1) [29] using a system of capillaries and a hand press (HiP Co.™, Pennsylvania, PA, USA, position 4 in Figure 1). The control system for gas supply was carried out by two high-pressure valves (HiP Co.™, Pennsylvania, PA, USA) (positions 3 and 6 in Figure 1) and connected by three-way two-stem hand valves (Top Industrie™, Vaux-le-Pénil, France, position 7 in Figure 1). Monitoring of the carbon dioxide pressure value in the system was carried out using an electronic pressure transmitters (Gems™, Basingstoke, UK, position 2, 5, 8 in Figure 1) with an accuracy of ±0.05 Mpa.

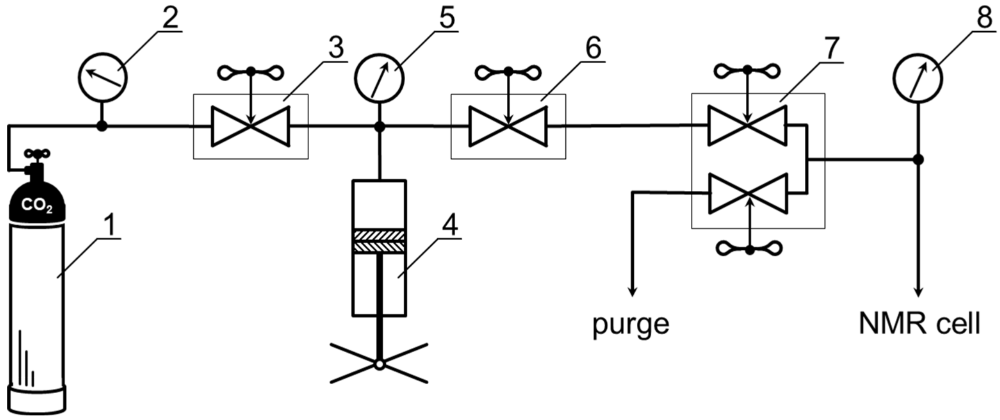

Figure 1. Scheme of the installation of high pressure equipment for creating and maintaining high pressure NMR experiments for the supercritical CO_2. 1—gas cylinde; 2,5,8—pressure transmitters; 3,6—high-pressure valves; 4—hand press; 7—hand valves.

The high-pressure equipment, together with a high-pressure NMR cell and a Bruker Avance III 500 spectrometer, makes it possible to record NMR spectra at pressures up to 30 Mpa and temperatures up to 90 °C. The standard ^{1}H NMR spectra of MFA (Figure S1) [30] were acquired with a spectral width 18 ppm, 32,768 data points, relaxation delay 2 s, and 512 scans. The ^{13}C NMR spectrum of MFA (Figure S2) was acquired with a spectral width 270 ppm, 65,336 data points, relaxation delay 2 s, and 4096 scans. The standard for chemical shifts (δ_{TMS} = 0 ppm) is dilute tetramethylsilane (TMS) in DMSO-d_6.

The ^{1}H-^{13}C Heteronuclear single quantum coherence spectroscopy (^{1}H-^{13}C HSQC) [31–34] (see Figure S3) and heteronuclear multiple-bond correlation spectroscopy (^{1}H-^{13}C HMBC) [35] (Figure S4) spectra were acquired in the phase-sensitive mode with 256 (F1) and 1024 (F2) data points, 32 for HSQC and 64 for HMBC scans per increment, spectral widths of 18 and 270 ppm in the ^{1}H and ^{13}C dimensions, respectively. ^{1}H-^{1}H Total Correlation Spectroscopy (^{1}H-^{1}H TOCSY) and Nuclear Overhauser Effect Spectroscopy (^{1}H-^{1}H NOESY) [36–39] spectra were acquired using two different spin locks (20 and 100 ms) and from five (DMSO-d_6-CO_2) to fifteen (DMSO-d_6 150-900 ms) different mixing time parameters [30,40] (see Figure S5 and S6) with 256 (F1) and 2048 (F2) data points, 16 scans per increment, and spectral widths of 18 ppm.

The values of the chemical shifts for ^{1}H and ^{13}C, assignment of groups of atoms for MEF, and the corresponding cross-peaks ^{1}H-^{13}C HSQC, ^{1}H-^{13}C HMBC, and ^{1}H-^{1}H TOCSY are given in the Table S1.

The temperature 45 °C and pressure 9 MPa of the high-pressure NMR experiment were set in accordance with the point 98:2 of the phase diagram of CO_2: DMSO-d_6 [41,42]. The choice of state parameters during NMR experiments is due primarily to the need to minimize the content in bulk of the DMSO-d_6. This ensures acceptable purity of the micronized particles and avoids the formation of co-solvents with DMSO. It should be noted that scCO_2 + DMSO-d_6 can be in a subcritical state at these state parameters [41,43].

Calculation of vibrational energies and frequencies of MFA conformers was carried out using the software package Gaussian (Gaussian16Wversion 1.1 Gaussian, Inc.,Wallingford, CT, USA) in the framework of density functional theory (DFT) by the "Becke, 3-parameter, Lee–Yang–Parr" (B3LYP) method with the 6-311+G(2d,p) basis set, which have proven themselves well in the conformational analysis of small molecules with cyclic fragments [44] and MFA, in particular [27]. The results of quantum chemical calculations made it possible to determine the energy values of conformers, the coordinates of atoms, as well as their magnetic shielding tensors (Tables S4–S10). The structure of each conformer corresponded to local energy minima and was confirmed by the absence of virtual (imaginary) frequencies. In addition, within the framework of quantum chemical calculations, the GIAO (gauge-independent atomic orbital) method was used to verify the obtained structures of MFA conformers. The magnetic shielding tensors of carbon atoms in the structure of molecules of various conformers have been determined and the values of chemical shifts have been calculated. A comparative analysis of the calculated (GIAO) and experimental (^{13}C NMR) values of chemical shifts made it possible to establish that their coefficients of determination (R^2) range from 0.996 to 0.999, which is an experimental confirmation of the correctness of the obtained conformer structures in the framework of DFT calculations [45].

3. Results and Discussion

3.1. An Analysis of Structure of MFA

Mefenamic acid (2-[(2,3-dimethylphenyl)amino]benzoic acid) is a derivative of anthranilic acid in which one of the hydrogens attached to the nitrogen atom is replaced by the 2,3-dimethylphenyl moiety. Figure 2 shows the molecular structure of MFA with the atom numbering used in this paper. The conformation of the MFA molecule can be described by two dihedral angles: $\tau_1[C_2\text{-}N\text{-}C_3\text{-}C_7]$, describing rotation of the benzene rings, and $\tau_2[O{=}C_1\text{-}C_{13}\text{-}C_6]$, showing the orientation of the carboxyl group.

In addition to τ_1, the angle $[C_{13}\text{-}C_2\text{-}N\text{-}C_3]$ is also considered in the literature devoted to conformers of mefenamic acid and other fenamates [28,46], which characterizes rotation of the phenyl groups relative to the HN-C_2 axis. We do not consider conformers arising due to changes in the angle $[C_{13}\text{-}C_2\text{-}N\text{-}C_3]$ because the relative energies of these conformers are too high. Note that in the conformers discussed here, the value of the angle $[C_{13}\text{-}C_2\text{-}N\text{-}C_3]$ varies within 1–3°.

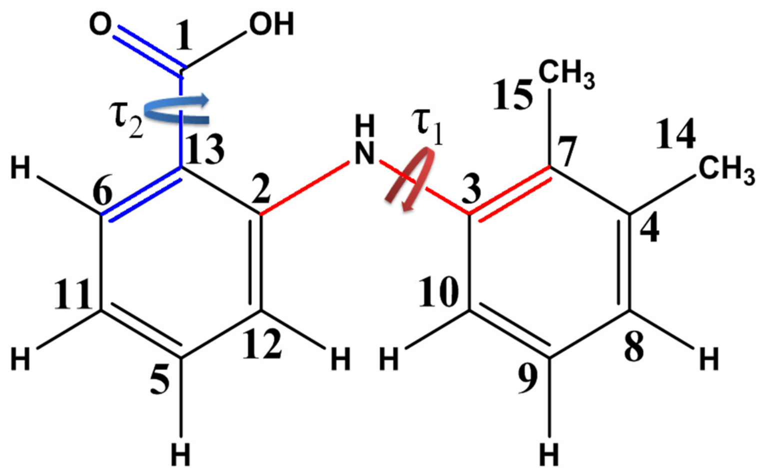

Figure 2. Structural formula of MFA. Atom numbering is used below for labeling signals and cross-peaks in NMR spectra and for denoting dihedral angles. Chemical bonds forming the dihedral angle $\tau_1[C_2\text{-}N\text{-}C_3\text{-}C_7]$ are shown in red; $\tau_2[O{=}C_1\text{-}C_{13}\text{-}C_6]$, in blue .

Carboxyl group and nitrogen atom in the molecule of mefenamic acid lie in one plane [47]. The sum of valence angles for all bonds linked to the nitrogen atom is close to 360°, so the sp^2 hybridization state may be suggested for the N atom. Three polymorphic forms of MFA are known today, termed forms I, II, and III [46,48]. As for other fenamates, polymorphism of MFA arises due to the molecule package and also their conformation. In particular, conformers comprising form I have the τ_1 angle equal to −119.99° (CH_3 groups pointing up in Figure 3), while in forms II and III, this angle is 68.20° and −80.82°, respectively (CH_3 groups pointing down in Figure 3) [46].

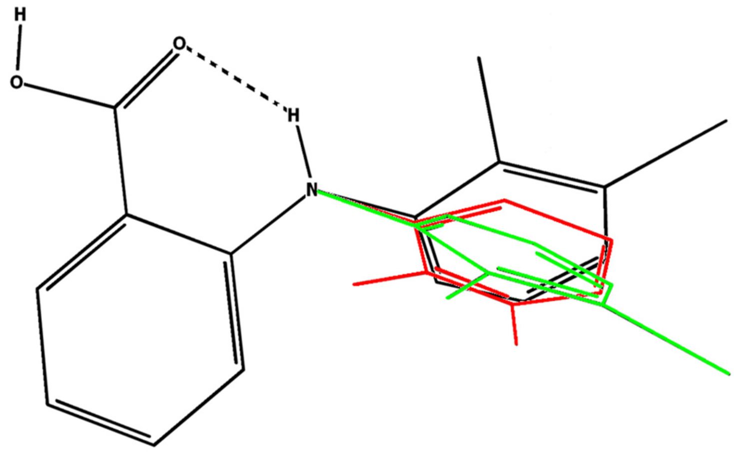

Figure 3. Structure of the MFA conformers present in polymorphic forms I (black) [49], II (red) [28], and III (green) [46].

Conformation of the molecules present in the MFA polymorphs is stabilized by an intramolecular hydrogen bond. Note that the structures I and II differ by the dihedral angle τ_1[C_2-N-C_3-C_7], the value of which can directly affect the energy of the crystal lattice [50]. Polymorphic form I is obtained by evaporating organic solutions in acetone and ethanol, and MFA II can be obtained by recrystallization of MFA I in dimethylformamide (DMF). Transition from MFA I to MFA II was shown to occur in the temperature range from 160 to 190 °C; the transition temperature depends on the heating rate or mechanical compressing of the solid material [51]. Polymorphic form III was described in [52]. To block the growth of crystals of the stable forms and to obtain MFA III, the authors used structurally related compounds affecting the nucleation and growth of host crystals. Quite possibly, the crystalline variability of MFA is not limited to these three polymorphic forms. For possible control of polymorphism during micronization (e.g., by the DELOS method [25]), conformation screening was performed using combined analysis of NMR experiments and quantum-chemical calculations. This information may be useful, since investigation of polymorphism in microscopic crystals is a difficult task requiring expensive instrumentation such as Flash DSC 1 (Flash Differential Scanning Calorimeter) setup for ultrafast calorimetry [53], and powder X-ray studies do not always distinguish different powders in a mix.

Quantum-chemical calculations predict the four most probable conformers of MFA, labeled from A to D in Figure 4. They differ both by the angle τ_1[C_2-N-C_3-C_7] and by τ_2[O=C_1-C_{13}-C_6], i.e., by mutual orientation of the benzene rings and carboxyl group. Calculations did not allow for the environment using the polarizable continuum model (PCM), because it might prevent some conformers from being found [54]. This might lead to erroneous or incomplete information on the conformational equilibrium.

The obtained set of most probable conformers was divided into groups following geometric criteria (angles and distance between protons). Thus, the angle τ_1 is −136.40° and −76.58° in the conformers A + C and B + D, respectively; these conformer groups differ by the positions of the benzene ring planes. The groups A + B and C + D have different angles τ_2: 176.12° and −5.37°, respectively (Figure 3). Note that deviation in the non-changing angles within each group was within 1.5°. Fractions of the mentioned groups were found using the NOESY data obtained in DMSO-d_6 (at 25 °C and 0.1 MPa) and in the $scCO_2$ + DMSO-d_6 medium (45 °C, 9 MPa).

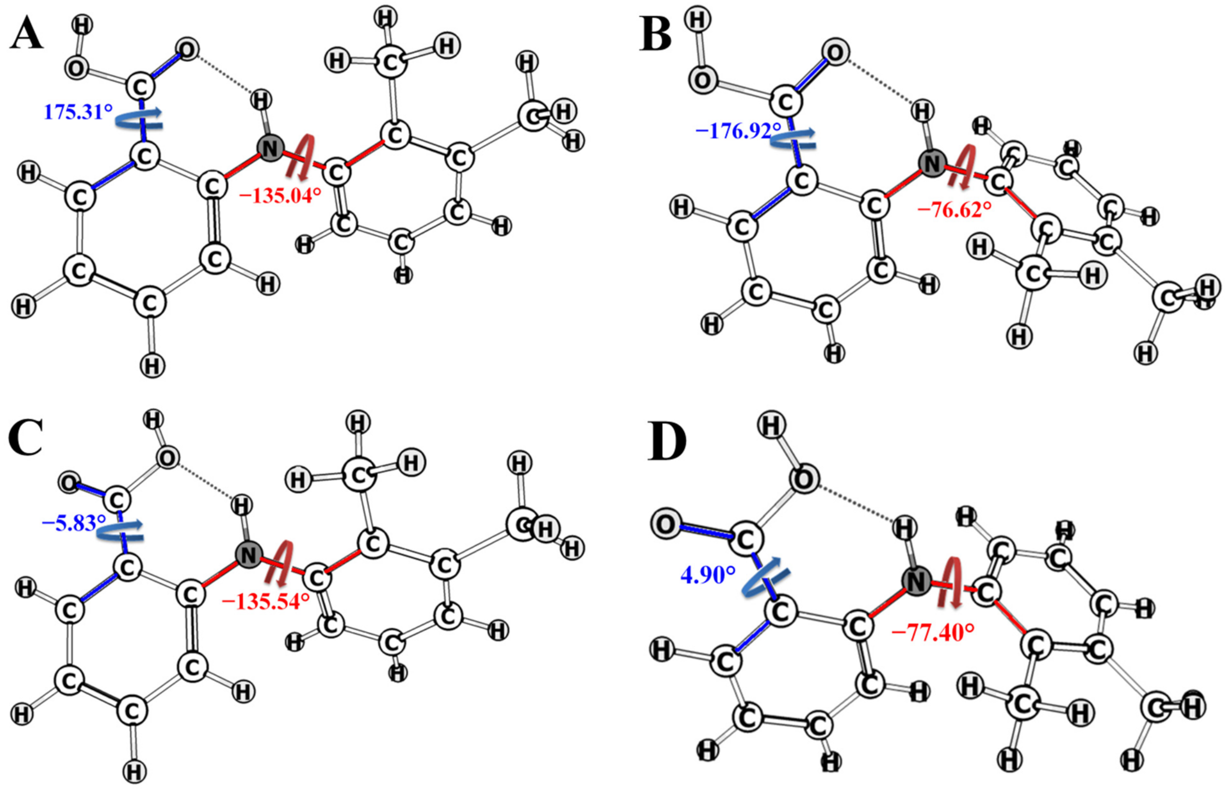

Figure 4. Structures of the MFA conformers and dihedral angles τ_1[C2-N-C3-C7] (red) and τ_2[O=C1-C13-C6] (blue).

Before performing the analysis of NOESY spectra, [1]H and [13]C NMR signals were assigned using 1D (Figures S1 and S2) and 2D NMR experiments [1]H-[13]C HSQC, [1]H-[13]C HMBC, and [1]H-[1]H TOCSY (Figures S3–S6). Then, assigned [1]H signals were used to analyze cross-peaks observed in the NOESY spectrum of MFA (Figure 5).

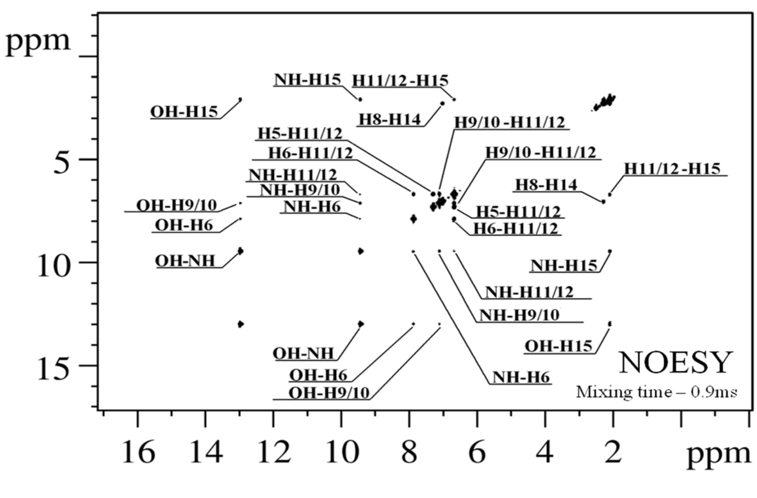

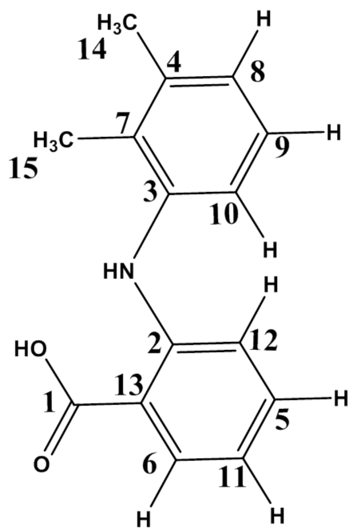

(**a**) (**b**)

Figure 5. [1]H-[1]H NOESY NMR spectrum of MFA in DMSO-d6 (**a**). Observed cross-peaks correspond to hydrogen atoms separated by a distance less than 5 Å. Atom numbering is shown in the right panel of the figure (**b**).

The cross-peaks in the NOESY spectrum correspond to 13 intramolecular proton–proton distances shorter than 5 Å. Corresponding distances were calculated based on the data of quantum-chemical calculations using appropriate averaging models for different types of intramolecular flexibility [55–58].

Analysis of the NOESY-detected distances shows that there are two atom pairs, the distance between which depends noticeably on conformational changes. These are H9/10-H11/12, sensitive to rotation of the benzene rings, and OH-H6, showing rotation of the carboxyl group. Calculated distance in the pair OH-H6 is 3.27 ± 0.01 Å in group A + B and 4.34 ± 0.01 Å in group C + D (Table 1). Calculated distance of H9/10-H11/12 is 3.14 ± 0.02 and 4.61 ± 0.02 Å in group A + C and B + D, respectively (Table 1). A somewhat bigger difference of 0.02 Å between conformers A and C or B and D is caused by non-planar distortion of the benzene rings. In the case of fast movement of protons, as in the case of H9/10-H11/12, the averaging model given by Equation (1) is used:

$$r_i^{eff} = \left(\left(\frac{1}{n_I n_S} \sum_i \frac{1}{r_i^3} \right)^2 \right)^{-\frac{1}{6}}, \tag{1}$$

where r^{eff} is the averaged internuclear distance taken from the conformer structures obtained in quantum-chemical calculations, n_I and n_S are the numbers of equivalent spins the atom groups I and S, and r_i is the distance between the spins in the considered groups.

Reference distance was used to calculate experimental values in the slope of the ISPA (isolated spin–pair approximation) model. The choice of the reference requires that it should be the same in different conformers (differing by 0.01 Å or less) and the nuclear Overhauser effect is not distorted by anisotropy of intramolecular motion [59–61]. Finally, the atom pair H6-H11/12 was chosen as the reference, having the distance of 2.76 Å (Table 1). This value agrees well with the X-ray structural analysis data on the polymorphs of MFA [28,46,49]. Average distance was calculated using Equation (2), allowing for slow intramolecular flexibility:

$$r_i^{eff} = \left(\frac{1}{n_I n_S} \sum_i \frac{1}{r_i^6} \right)^{-\frac{1}{6}}, \tag{2}$$

Table 1. Conformation-dependent distances in the MFA conformers based on quantum-chemical calculations.

Interproton Distances, Å	Conformers			
	A	B	C	D
H9/10-H11/12	3.12	4.64	3.16	4.59
OH-H6	3.27	3.28	4.34	4.34
H6-H11/12	2.77	2.77	2.78	2.78

Distances H9/10-H11/12 and OH-H6 were determined from NOESY experiments to calculate the fraction of the MFA conformer groups. The approach for determination of the distance relies on the fact that the cross-relaxation rate depends on the distance between the nuclei, as given by Equation (3):

$$\sigma_{ij} = \frac{1}{{r_{ij}}^{6}}, \tag{3}$$

where σ_{ij} is the cross-relaxation rate between nuclei *i* and *j*, and r_{ij} is the distance between them. Having known one fixed internuclear distance, we determined all other distance values using the ISPA model [29,54,62] (see Equation (4) below).

The cross-relaxation rates found from the NOE data for the atom groups H9/10-H11/12, OH-H6 and H6-H11/12 obtained in DMSO-d_6 were found to be (1.57 ± 0.02) × 10^{-2}, (1.28 ± 0.09) × 10^{-2}, and (3.34 ± 0.02) × 10^{-2} s^{-1}, respectively. In the measurements carried out in $scCO_2$ + DMSO-d_6 at 45 °C and 9 MPa, the corresponding cross-relaxation rates were (1.56 ± 0.09) × 10^{-2}, (0.99 ± 0.08) × 10^{-2}, and (4.18 ± 0.3) × 10^{-2} s^{-1}.

Distances obtained using Equation (4) (ISPA) for the atom pairs H9/10-H11/12 and OH-H6 for MFA in DMSO-d_6 were found to be 3.13 ± 0.009 and 3.24 ± 0.04 Å, respectively; for MFA in the mixed solvent, they were 3.25 ± 0.06 and 3.51 ± 0.09 Å, respectively.

$$r_{\exp} = r_0 \left(\frac{\sigma_0}{\sigma_{\exp}} \right)^{\frac{1}{6}}, \tag{4}$$

where r_0 is the reference distance obtained from X-ray experiments, σ_0 is the measured cross-relaxation rate for the reference atom pair, and $\sigma_{\exp}$ is the cross-relaxation rate for the distance to be determined from NOESY data.

Lee and Krishna showed that in the case of fast conformational exchange, the observed cross-relaxation rate is an average of the rates corresponding to individual conformers (see Equation (5)) [63]. Hence, the distance will also be averaged. The cross-relaxation rate can be found from linear approximation of the dependence $I_{ij}(\tau_m)$ of the integral intensity of the NOESY cross-peaks (Equation (6)) on the mixing time parameter, τ_m, of the NMR experiment. To find the cross-relaxation rates of the conformation-dependent and reference distances, we recorded a set of NOESY spectra where the mixing time varied from 0.15 to 0.9 s. The slope of the obtained dependences allowed determination of the σ values (Figure 6). The raw data for building the plots and corresponding cross-relaxation rates and their inaccuracies are listed in Tables S2 and S3.

$$\sigma_{\exp} = \sum_i \sigma_i x_i, \tag{5}$$

where σ is the resulting average cross-relaxation rate, σ_i is the cross-relaxation rate in the conformer *i*, and x_i is the relative fraction of this conformer.

$$I_{ij}(\tau_m) = \frac{1}{2}\left(\frac{1}{n_j}\left| \frac{a_{ij}(\tau_m)}{a_{ii}(\tau_m)} \right| + \frac{1}{n_i}\left| \frac{a_{ji}(\tau_m)}{a_{jj}(\tau_m)} \right| \right), \tag{6}$$

where n_j and n_i are the number of protons within the considered group of equivalent atoms, and a_{ij} and a_{ji} are the parameters showing the intensity of 2D NOESY cross-peaks.

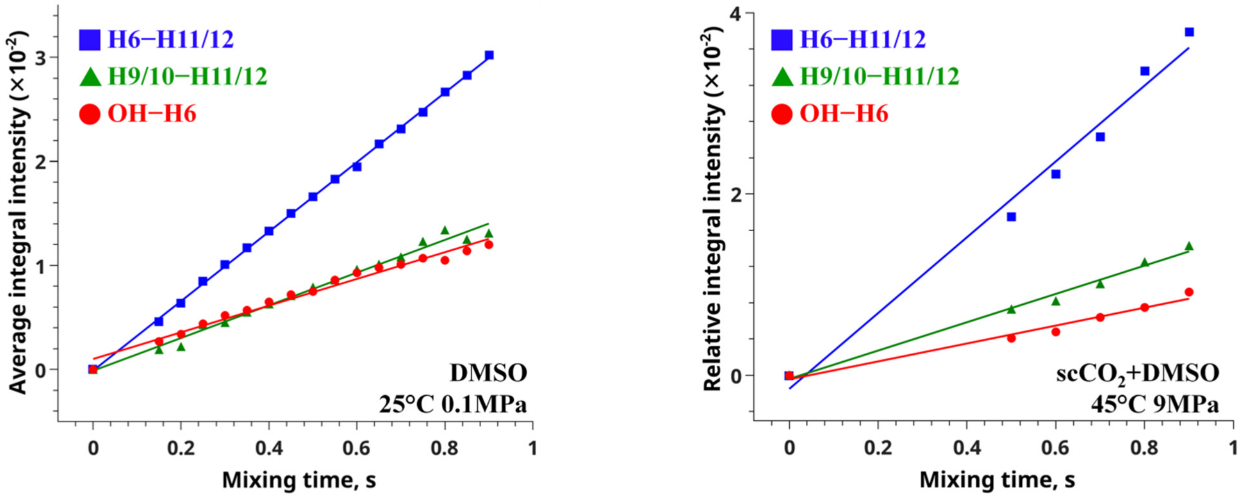

(**a**) (**b**)

Figure 6. Integral intensity as a function of the mixing time for the conformation-dependent (red and green lines) and reference (blue) distances, obtained by analysis of NOESY spectra measured for MFA in DMSO-d$_6$ (**a**) and $scCO_2$+DMSO-d$_6$ at 45°, 9 MPa (**b**).

By substituting the obtained values into the Equation (7) of two-position exchange, we built a plot of the difference between the calculated and experimental distances as a function of the conformer fractions (Figure 7b). The inaccuracy level of determination of the experimental distance for MFA in DMSO-d$_6$ was also plotted in the figure [29,64,65].

$$\frac{1}{r_{\exp}^{6}} = \frac{x_1}{r_1^6} + \frac{1-x_1}{r_2^6} \rightarrow x_1 = \frac{r_1^6\left(r_2^6 - r_{\exp}^6\right)}{r_{\exp}^6\left(r_2^6 - r_1^6\right)}, \tag{7}$$

where r_{exp} is the experimental distance determined from NOESY, and r_1 and r_2 are the distances between the atoms in individual conformers.

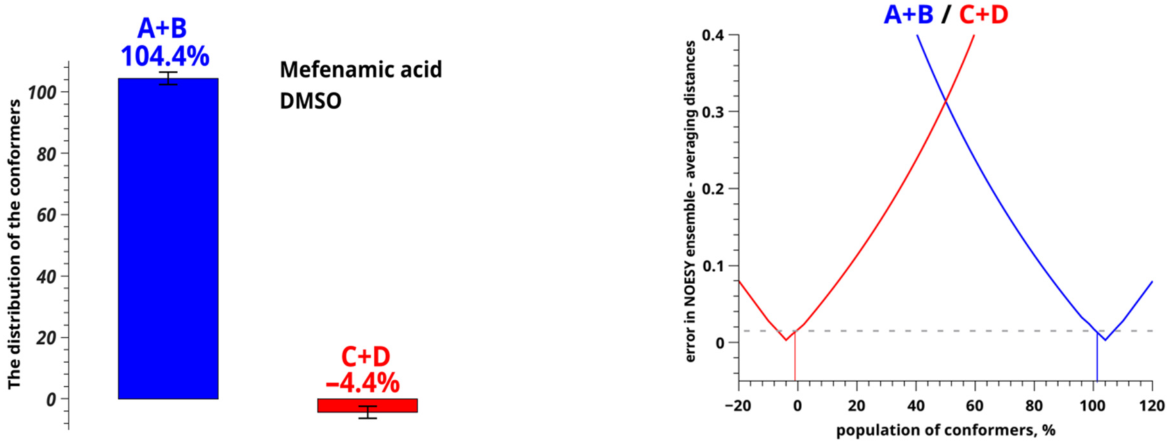

(**a**) (**b**)

Figure 7. Distribution (**a**) and population (**b**) of conformers of MFA in DMSO-d$_6$ calculated from the observed conformation-dependent distance OH-H6.

3.2. Influence of Hidden Conformers of MFA in DMSO-d$_6$

Relative equilibrium fractions of MFA conformers in DMSO-d$_6$ were determined following Equation (7); results are shown in Figure 7a.

Minimums of the plot (Figure 7b) correspond to the populations of the conformer groups (blue and red curves); dashed gray line shows the error level of determining the distances. Crossing of the solid and dashed lines shows the conformer fraction ranges [55,66,67].

Evidently, the predicted fractions of the conformer groups related to variation of the angle τ_2[O=C_1-C_{13}-C_6] for MFA in pure DMSO-d_6 are meaningless: 104.4 ± 2% for A + B and −4.4 ± 2% for C + D. This may be caused by the fact that some of the conformers have been omitted from the analysis. Thus, two new conformers were added (called AA and BB), in which the variation of the angle τ_3[O=C_1-O-H] (mobility of the hydroxyl group) is taken into account. The angle τ_3 is 170.66° in AA and −171.35° in BB (Figure 8). This type of molecular rearrangement seemed unlikely, and the necessity to add new forms into the analysis was unexpected.

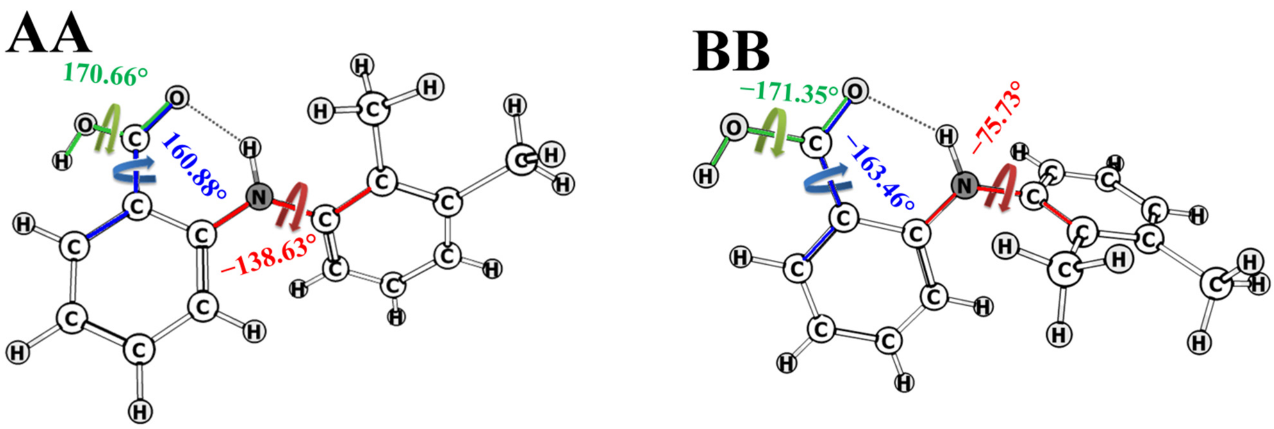

(**a**) (**b**)

Figure 8. Structure of MFA conformers AA (**a**) and BB (**b**) and dihedral angles τ_1[C_2-N-C_3-C_7] (red), τ_2[O=C_1-C_{13}-C_6] (blue), and τ_3[O=C_1-O-H] (green arrow).

Conformation-dependent distance OH-H6 for these conformers was calculated to be 1.89 Å in AA and 1.86 Å in BB; the value of H9/H10-H11/H12 is 3.08 and 4.65 Å, respectively. According to the geometric criteria, we consider conformer groups A + C + AA and B + D + BB when rotation of the angle τ_1[C_2-N-C_3-C_7] takes place (rotation of the benzene rings), and groups A + B+AA + BB with C + D when the angle τ_2[O=C_1-C_{13}-C_6] changes (rotation of the carboxyl group). A new group was also added for separate estimating the fraction of conformer groups A + B and AA + BB, in which the angle τ_3[O=C_1-O-H] (flexibility of the hydroxyl group) is the criterion. The distance H9/10-H11/12 in the groups A + C + AA is 3.12 Å, and in B + D + BB, it is 4.62 Å. The distance OH-H6 takes the following values: 2.09 Å in A + B + AA + BB, 4.34 Å in C + D, 3.27 Å in A + B, and 1.88 Å in AA + BB. Using the above-mentioned method of analysis of the NOESY data within the ISPA model and assuming the two-position exchange, we calculated the populations of the groups A + B + AA + BB and C + D for MFA in DMSO-d_6. They were found to be 6.3 ± 1% and 93.9 ± 1%, respectively (Figure 9).

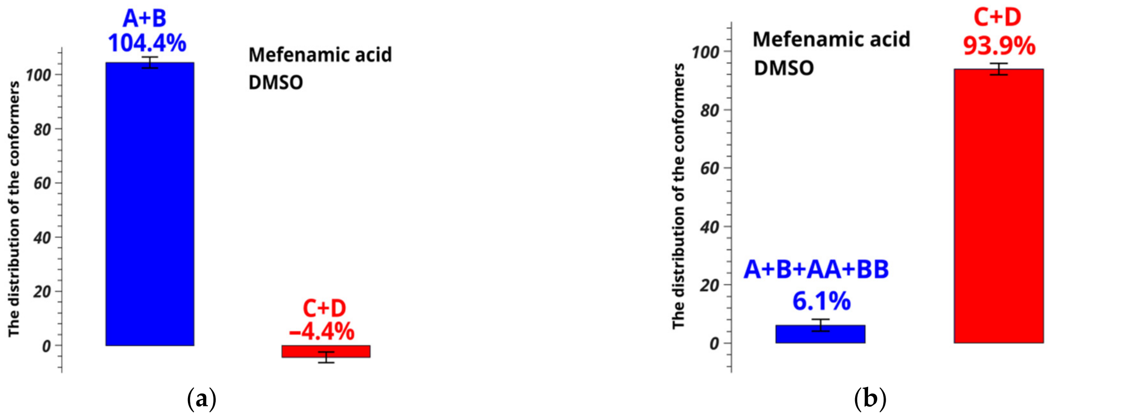

Figure 9. Distribution of conformers of MFA in DMSO-d_6 calculated from the observed conformation-dependent distance OH-H6 (**a**) without and (**b**) allowing for the existence of additional conformers AA and BB. Figure 9a is a duplicate of Figure 7a for comparison.

Figure 9 shows that neglecting the intramolecular lability of the hydroxyl group and omitting hidden conformers leads to wrong conclusions and the error of 98.1% in numerical interpretation of NOESY results.

3.3. Influence of Hidden Conformers of MFA in $scCO_2$

At the next step, populations of the conformer groups related to the mobility of the carboxyl group (angle τ_2[O=C_1-C_{13}-C_6]) in the mixed solvent $scCO_2$ + DMSO-d_6 at 45 °C and 9 MPa were determined. Results of the calculations are presented in Figure 10.

Choice of these particular parameters of state is justified by the fact that increasing the pressure to 10 MPa at the same temperature of 45 °C brings the system $scCO_2$ + DMSO-d_6 to the critical point [43]. It is accompanied by substantial density fluctuations with minimal variations of pressure, and NMR spectra of high quality cannot be recorded any more. Use of the pressure below 9 MPa or other temperatures results in an increase in the molar fraction of DMSO-d_6, which is also undesirable because it can cause formation of crystal solvates.

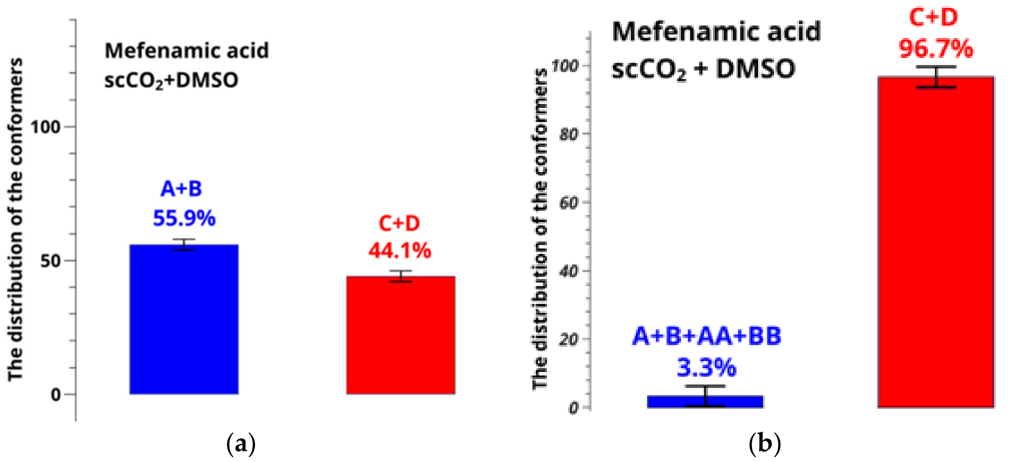

Figure 10. Distribution of conformers of MFA in $scCO_2$ + DMSO-d_6 at 9 MPa calculated from the observed conformation-dependent distance OH-H6 (**a**) without and (**b**) allowing for the existence of additional conformers AA and BB.

Comparison of the results shown in Figure 10 leads us to a conclusion that the error in determining the conformer fractions in the case of the mixed solvent is also very large, exceeding 50%. Thus, using the model of two-position chemical exchange given by Equation (6) and allowing for the additional conformers, we plotted the dependences of the difference between the calculated and experimental distances on the conformer group fractions, which finally gave the conformer group populations (Figure S7). Thus, new conformer fractions were found, allowing the motions of the hydroxyl group for MFA dissolved in DMSO-d_6 at 25 °C and mixed solvent $scCO_2$ + DMSO-d_6 at 45 °C and 9 MPa; results are summarized in Figure 11.

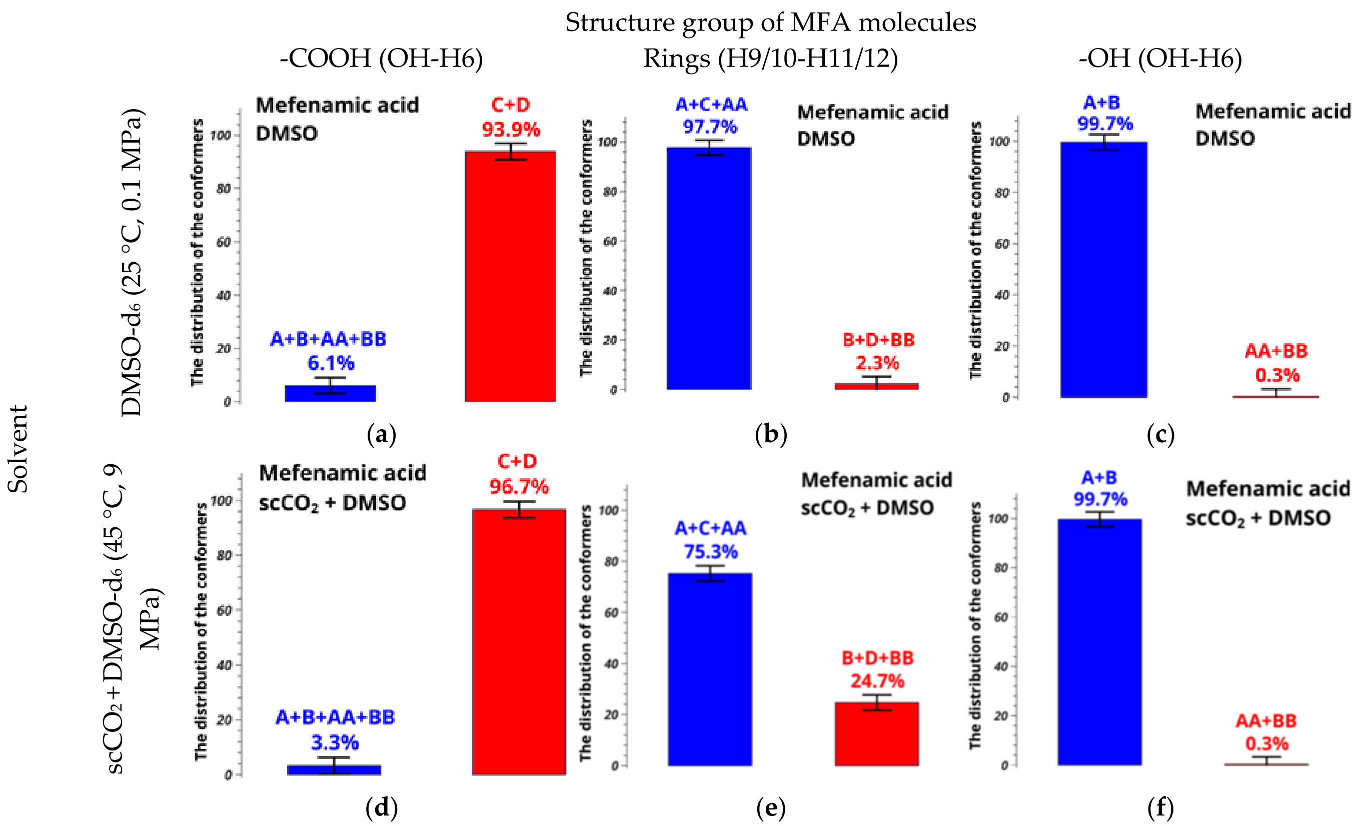

Figure 11. Relative conformer group fractions of MFA in (**a**–**c**) DMSO-d_6 and (**d**–**f**) $scCO_2$ + DMSO at supercritical parameters of state, calculated from experimentally found distances OH-H6 and H9/10-H11/12.

Although the populations of conformers AA + BB are very small, only approximately 0.3%, including them in the NOESY data analysis is crucial to obtaining correct results on the conformer populations. If an incomplete set of conformers is considered [68], numerical results and conclusions become incorrect. All distance values given by quantum-chemical calculations and experimental ones are listed in Tables S2 and S3.

The fraction of the group A + C + AA decreases significantly (and that of B + D + BB grows), by 22.4%, as we go from the system in pure DMSO-d_6 to the mixed solvent based on $scCO_2$. Since the molar fraction of DMSO-d_6 in $scCO_2$ in our experimental conditions is only 2%, the main effect should be caused by addition of carbon dioxide. For example, addition of $scCO_2$ may diminish the solvation effect of DMSO-d_6 onto MFA; consequently, the number of intermolecular interactions also decreases, and this leads to redistribution of the conformer fractions in the solvent $scCO_2$ + DMSO-d_6. We suppose that the obtained relative conformer populations in the mixed solvent should be close to that existing in pure $scCO_2$.

Diagrams shown in Figure 11 demonstrate that the fraction of A + C + AA decreases by 22.4% (rotation of the benzene rings) upon addition of $scCO_2$. At the same time, the fractions of groups A + B + AA + BB and C + D, as well as A + B and AA + BB, experience smaller modifications, within 2.9%. In general, the group A + C + AA dominates in the system, which facilitates formation of the stable polymorphic form I.

4. Conclusions

Preferred conformers of mefenamic acid dissolved in DMSO-d_6 (at 25 °C and 0.1 MPa) and in the mixed medium $scCO_2$ + DMSO-d_6 (45 °C, 9 MPa) were determined. Hidden conformers, which are not observed directly in the NOESY spectra, were shown to be important for correct calculation of the conformer fractions. Redistribution of the conformer group populations upon addition of supercritical carbon dioxide was revealed. Use of DMSO-d_6 as a co-solvent in $scCO_2$ allows determination of the conformation distribution of compounds poorly soluble in pure $scCO_2$, including fenamates. Obtained results may be of use in design and practical implementation of the drug micronization process. In future perspectives, we would like to conduct the comparison of structural features of different fenamates [69] and lidocaine [64,70]. It should elucidate the question of whether addition of DMSO has a certain effect on the conformational equilibrium. In future works, it would be interesting to study the effect of the attendance of a trifluoromethyl substituted fragment in fenamates [71] (for example, flufenamic acid) on conformational equilibria in $scCO_2$.

Supplementary Materials: The following supporting information can be downloaded at: https://www.mdpi.com/article/10.3390/pharmaceutics14112276/s1. The ^{1}H and ^{13}C NMR spectra, ^{1}H-^{13}C HSQC, ^{1}H-^{13}C HMBC, ^{1}H-^{1}H TOCSY (spin-locks with 20 and 100 ms) of MFA in DMSO-d_6. **(**Figures S1–S6**).** The plots of populations of the conformer groups (Figure 7). The chemical shift of the ^{1}H and ^{13}C nuclei is determined by 2D spectra of the MFA molecule (Table S1). Normalized integral intensities of the cross-peaks, cross-relaxation rates, and proton–proton distances in the MFA molecule (Tables S2–S3). The energy value, structure, coordinates of atoms, and the values of their magnetic shielding obtained from the data of quantum chemical calculations for all conformers of MFA (Tables S4–S10).

Author Contributions: K.V.B.: formal analysis, writing—review and editing, investigation, and visualization; L.A.E.B.d.C.: conceptualization, investigation, formal analysis, validation, data curation, and writing—review and editing; A.A.D.: methodology, formal analysis, and investigation; S.V.E.: investigation, formal analysis, validation, and writing—review and editing; I.A.K.: conceptualization, methodology, investigation, formal analysis, validation, writing—original draft, writing—review and editing, project administration, and funding acquisition. All authors have read and agreed to the published version of the manuscript.

Funding: The research is supported by the grant of the Russian Science Foundation (project no. 22-23-00793).

Institutional Review Board Statement: Not applicable.

Informed Consent Statement: Not applicable.

Data Availability Statement: Not applicable.

Acknowledgments: Authors dedicate this research to the memory of M.Yu. Nikiforov, who inspired this work. L.A.E.B.d.C. appreciates the Molecular Physical-Chemistry R&D Unit of University of Coimbra (Portuguese Foundation for Science and Technology (FCT) contracts UIDB/00070/2020 & UIDP/00070/2020) for the quantum-chemistry analysis.

Conflicts of Interest: The authors declare no conflict of interest.

References

1. Jin, G.; Wong, S.T.C. Toward Better Drug Repositioning: Prioritizing and Integrating Existing Methods into Efficient Pipelines. *Drug Discov. Today* **2014**, *19*, 637–644. https://doi.org/10.1016/J.DRUDIS.2013.11.005.
2. Zheng, W.; Sun, W.; Simeonov, A. Drug Repurposing Screens and Synergistic Drug-Combinations for Infectious Diseases. *Br. J. Pharmacol.* **2018**, *175*, 181–191. https://doi.org/10.1111/BPH.13895.
3. Andreas Papapetropoulos, C.; Papapetropoulos, A.; Szabo, C. Inventing New Therapies without Reinventing the Wheel: The Power of Drug Repurposing. *Br. J. Pharmacol.* **2018**, *175*, 165–167. https://doi.org/10.1111/BPH.14081.
4. Debnath, A.; Parsonage, D.; Andrade, R.M.; He, C.; Cobo, E.R.; Hirata, K.; Chen, S.; García-Rivera, G.; Orozco, E.; Martínez, M.B.; et al. A High-Throughput Drug Screen for Entamoeba Histolytica Identifies a New Lead and Target. *Nat. Med.* **2012**, *18*, 956–960. https://doi.org/10.1038/nm.2758.

5. Harbut, M.B.; Vilchèze, C.; Luo, X.; Hensler, M.E.; Guo, H.; Yang, B.; Chatterjee, A.K.; Nizet, V.; Jacobs, W.R.; Schultz, P.G.; et al. Auranofin Exerts Broad-Spectrum Bactericidal Activities by Targeting Thiol-Redox Homeostasis. *Proc. Natl. Acad. Sci. USA* **2015**, *112*, 4453–4458.
6. Xu, M.; Lee, E.M.; Wen, Z.; Cheng, Y.; Huang, W.K.; Qian, X.; Tcw, J.; Kouznetsova, J.; Ogden, S.C.; Hammack, C.; et al. Identification of Small-Molecule Inhibitors of Zika Virus Infection and Induced Neural Cell Death via a Drug Repurposing Screen. *Nat. Med.* **2016**, *22*, 1101–1107. https://doi.org/10.1038/nm.4184.
7. Cimolai, N. The Potential and Promise of Mefenamic Acid. *Expert Rev. Clin. Pharmacol.* **2013**, *6*, 289–305. https://doi.org/10.1586/ecp.13.15.
8. Myles, A.B.; Bacon, P.A.; Williams, K.A. Mefenamic Acid in Rheumatoid Arthritis. *Ann. Rheum. Dis.* **1967**, *26*, 494–498. https://doi.org/10.1136/ARD.26.6.494.
9. Khan, M.S.Y.; Akhter, M. Glyceride Derivatives as Potential Prodrugs: Synthesis, Biological Activity and Kinetic Studies of Glyceride Derivatives of Mefenamic Acid. *Pharmazie* **2005**, *60*, 110–114.
10. Kim, J.H.; Jung, J.Y.; Shim, J.H.; Kim, J.; Choi, K.H.; Shin, J.A.; Choi, E.S.; Lee, S.O.; Chintharlapalli, S.; Kwon, K.H.; et al. Apoptotic Effect of Tolfenamic Acid in KB Human Oral Cancer Cells: Possible Involvement of the p38 MAPK Pathway. *J. Clin. Biochem. Nutr.* **2010**, *47*, 74–80. https://doi.org/10.3164/jcbn.10-02.
11. Ho Woo, D.; Han, I.-S.; Jung, G. Mefenamic Acid-Induced Apoptosis in Human Liver Cancer Cell-Lines through Caspase-3 Pathway. *Life Sci.* **2004**, *75*, 2439–2449. https://doi.org/10.1016/j.lfs.2004.04.042.
12. Zhu, W.; Smith, A.; Young, C.Y.F. A Nonsteroidal Anti-Inflammatory Drug, Flufenamic Acid, Inhibits the Expression of the Androgen Receptor in LNCaP Cells. *Endocrinology* **1999**, *140*, 5451–5454. https://doi.org/10.1210/ENDO.140.11.7246.
13. Charoenchaitrakool, M.; Dehghani, F.; Foster, N.R.; Chan, H.K. Micronization by Rapid Expansion of Supercritical Solutions to Enhance the Dissolution Rates of Poorly Water-Soluble Pharmaceuticals. *Ind. Eng. Chem. Res.* **2000**, *39*, 4794–4802. https://doi.org/10.1021/ie000151a.
14. Bolten, D.; Türk, M. Micronisation of Carbamazepine through Rapid Expansion of Supercritical Solution (RESS). *J. Supercrit. Fluids* **2012**, *62*, 32–40. https://doi.org/10.1016/J.SUPFLU.2011.06.014.
15. Türk, M.; Bolten, D. Polymorphic Properties of Micronized Mefenamic Acid, Nabumetone, Paracetamol and Tolbutamide Produced by Rapid Expansion of Supercritical Solutions (RESS). *J. Supercrit. Fluids* **2016**, *116*, 239–250. https://doi.org/10.1016/j.supflu.2016.06.001.
16. Shariati, A.; Peters, C.J. Recent Developments in Particle Design Using Supercritical Fluids. *Curr. Opin. Solid State Mater. Sci.* **2003**, *7*, 371–383. https://doi.org/10.1016/J.COSSMS.2003.12.001.
17. Sekhon, B.S. Supercritical Fluid Technology: An Overview of Pharmaceutical Applications. *Int. J. PharmTech Res.* **2010**, *2*, 810–826.
18. Martin Del Valle, E.M.; Galan, M.A. Supercritical Fluid Technique for Particle Engineering: Drug Delivery Applications. *Rev. Chem. Eng.* **2005**, *21*, 33–69. https://doi.org/10.1515/REVCE.2005.21.1.33.
19. Padrela, L.; Rodrigues, M.A.; Velaga, S.P.; Fernandes, A.C.; Matos, H.A.; de Azevedo, E.G. Screening for Pharmaceutical Cocrystals Using the Supercritical Fluid Enhanced Atomization Process. *J. Supercrit. Fluids* **2010**, *53*, 156–164. https://doi.org/10.1016/J.SUPFLU.2010.01.010.
20. Jessop, P.G.; Subramaniam, B. Gas-Expanded Liquids. *Chem. Rev.* **2007**, *107*, 2666–2694. https://doi.org/10.1021/CR040199O.
21. Foster, N.; Mammucari, R.; Dehghani, F.; Barrett, A.; Bezanehtak, K.; Coen, E.; Combes, G.; Meure, L.; Ng, A.; Regtop, H.L.; et al. Processing Pharmaceutical Compounds Using Dense Gas Technology. *Ind. Eng. Chem. Res.* **2003**, *42*, 6476–6493. https://doi.org/10.1021/ie030219x.
22. Zeinolabedini Hezave, A.; Khademi, M.H.; Esmaeilzadeh, F. Measurement and Modeling of Mefenamic Acid Solubility in Supercritical Carbon Dioxide. *Fluid Phase Equilib.* **2012**, *313*, 140–147. https://doi.org/10.1016/J.FLUID.2011.09.031.
23. Banchero, M.; Manna, L. Solubility of Fenamate Drugs in Supercritical Carbon Dioxide by Using a Semi-Flow Apparatus with a Continuous Solvent-Washing Step in the Depressurization Line. *J. Supercrit. Fluids* **2016**, *107*, 400–407. https://doi.org/10.1016/j.supflu.2015.10.008.
24. Tsai, C.C.; Lin, H.M.; Lee, M.J. Phase Equilibrium and Micronization for Flufenamic Acid with Supercritical Carbon Dioxide. *J. Taiwan Inst. Chem. Eng.* **2017**, *72*, 19–28. https://doi.org/10.1016/j.jtice.2017.01.011.
25. Ventosa, N.; Sala, S.; Veciana, J.; Torres, J.; Llibre, J. Depressurization of an Expanded Liquid Organic Solution (DELOS): A New Procedure for Obtaining Submicron- Or Micron-Sized Crystalline Particles. *Cryst. Growth Des.* **2001**, *1*, 299–303. https://doi.org/10.1021/CG0155090.
26. Chen, H.H.; Su, C.S.; Liu, J.J.; Sheu, M.T. Solid-State Property Modification and Dissolution Rate Enhancement of Tolfenamic Acid by Supercritical Antisolvent Process. *J. Supercrit. Fluids* **2015**, *101*, 17–23. https://doi.org/10.1016/j.supflu.2015.02.031.
27. Oparin, R.D.; Vaksler, Y.A.; Krestyaninov, M.A.; Idrissi, A.; Shishkina, S.V.; Kiselev, M.G. Polymorphism and Conformations of Mefenamic Acid in Supercritical Carbon Dioxide. *J. Supercrit. Fluids* **2019**, *152*, 104547. https://doi.org/10.1016/j.supflu.2019.104547.
28. Abbas, N.; Oswald, I.D.H.; Pulham, C.R. Accessing Mefenamic Acid Form II through High-Pressure Recrystallisation. *Pharmaceutics* **2017**, *9*, 16. https://doi.org/10.3390/pharmaceutics9020016.
29. Khodov, I.; Dyshin, A.; Efimov, S.; Ivlev, D.; Kiselev, M. High-Pressure NMR Spectroscopy in Studies of the Conformational Composition of Small Molecules in Supercritical Carbon Dioxide. *J. Mol. Liq.* **2020**, *309*, 113113. https://doi.org/10.1016/j.molliq.2020.113113.

30. Liu, M.; Mao, X.-A.; Ye, C.; Huang, H.; Nicholson, J.K.; Lindon, J.C. Improved Watergate Pulse Sequences for Solvent Suppression in NMR Spectroscopy. *J. Magn. Reson.* **1998**, *132*, 125–129. https://doi.org/10.1006/jmre.1998.1405.
31. Kalmykov, P.A.; Khodov, I.A.; Klochkov, V.V.; Klyuev, M.V. Theoretical and Experimental Study of Imine-Enamine Tautomerism of Condensation Products of Propanal with 4-Aminobenzoic Acid in Ethanol. *Russ. Chem. Bull.* **2017**, *66*, 70–75. https://doi.org/10.1007/s11172-017-1701-3.
32. Palmer, A.G., III.; Cavanagh, J.; Wright, P.E.; Rance, M. Sensitivity Improvement in Proton-Detected Two-Dimensional Heteronuclear Correlation NMR Spectroscopy. *J. Magn. Reson.* **1991**, *93*, 151–170. https://doi.org/10.1016/0022-2364(91)90036-S.
33. Kay, L.; Keifer, P.; Saarinen, T. Pure Absorption Gradient Enhanced Heteronuclear Single Quantum Correlation Spectroscopy with Improved Sensitivity. *J. Am. Chem. Soc.* **1992**, *114*, 10663–10665. https://doi.org/10.1021/ja00052a088.
34. Schleucher, J.; Schwendinger, M.; Sattler, M.; Schmidt, P.; Schedletzky, O.; Glaser, S.J.; Sørensen, O.W.; Griesinger, C. A General Enhancement Scheme in Heteronuclear Multidimensional NMR Employing Pulsed Field Gradients. *J. Biomol. NMR* **1994**, *4*, 301–306. https://doi.org/10.1007/BF00175254.
35. Cicero, D.O.; Barbato, G.; Bazzo, R. Sensitivity Enhancement of a Two-Dimensional Experiment for the Measurement of Heteronuclear Long-Range Coupling Constants, by a New Scheme of Coherence Selection by Gradients. *J. Magn. Reson.* **2001**, *148*, 209–213. https://doi.org/10.1006/jmre.2000.2234.
36. Kobchikova, P.P.; Efimov, S.V.; Khodov, I.A.; Klochkov, V.V. Features of Spatial Structures of Cyclosporins D, E and G Revealed by NMR and MD Simulations. *J. Mol. Liq.* **2021**, *336*, 116244. https://doi.org/10.1016/J.MOLLIQ.2021.116244.
37. Nikitina, L.E.; Pavelyev, R.S.; Startseva, V.A.; Kiselev, S.V.; Galiullina, L.F.; Aganova, O.V.; Timerova, A.F.; Boichuk, S.V.; Azizova, Z.R.; Klochkov, V.V.; et al. Structural Details on the Interaction of Biologically Active Sulfur-Containing Monoterpenoids with Lipid Membranes. *J. Mol. Liq.* **2020**, *301*, 112366. https://doi.org/10.1016/j.molliq.2019.112366.
38. Mamardashvili, G.M.; Kaigorodova, E.Y.; Khodov, I.A.; Scheblykin, I.; Mamardashvili, N.Z.; Koifman, O.I. Micelles Encapsulated Co(III)-tetra(4-Sulfophenyl)porphyrin in Aqueous CTAB Solutions: Micelle Formation, Imidazole Binding and Redox Co(III)/Co(II) Processes. *J. Mol. Liq.* **2019**, *293*, 111471. https://doi.org/10.1016/j.molliq.2019.111471.
39. Khodov, I.A.; Belov, K.V.; Krestyaninov, M.A.; Kiselev, M.G. Conformational Equilibria of a Thiadiazole Derivative in Solvents of Different Polarities: An NMR Study. *Russ. J. Phys. Chem. A* **2022**, *96*, 765–772. https://doi.org/10.1134/S0036024422040148.
40. Bax, A.D.; Davis, D.G. MLEV-17-Based Two-Dimensional Homonuclear Magnetization Transfer Spectroscopy. *J. Magn. Reson.* **1985**, *65*, 355–360. https://doi.org/10.1016/0022-2364(85)90018-6.
41. Andreatta, A.E.; Florusse, L.J.; Bottini, S.B.; Peters, C.J. Phase Equilibria of Dimethyl Sulfoxide (DMSO) + Carbon Dioxide, and DMSO + Carbon Dioxide + Water Mixtures. *J. Supercrit. Fluids* **2007**, *42*, 60–68. https://doi.org/10.1016/j.supflu.2006.12.015.
42. Lias, S.G.; Rosenstock, H.M.; Draxl, K.; Steiner, B.W.; Herron, J.T.; Holmes, J.L.; Levin, R.D.; Liebman, J.F.; Kafafi, S.A. Ionization Energetics Data, NIST Chemistry WebBook, NIST Standard Reference Database Number 69. *Natl. Inst. Stand. Technol. Gaithersbg. MD* **2011**, *20899*. https://doi.org/10.18434/T4D303.
43. Jaxel, J.; Gusenbauer, C.; Böhmdorfer, S.; Liebner, F.; Hansmann, C. Improving Single-Step scCO2 Dyeing of Wood by DMSO-Induced Micro-Swelling. *J. Supercrit. Fluids* **2020**, *165*, 104978. https://doi.org/10.1016/J.SUPFLU.2020.104978.
44. Aliev, A.E.; Courtier-Murias, D. Conformational Analysis of L-Prolines in Water. *J. Phys. Chem. B* **2007**, *111*, 14034–14042.
45. Khodov, I.A.; Belov, K.V.; Efimov, S.V.; Batista de Carvalho, L.A.E. Determination of Preferred Conformations of Mefenamic Acid in DMSO by NMR Spectroscopy and GIAO Calculation. *AIP Conf. Proc.* **2019**, *2063*, 040007. https://doi.org/10.1063/1.5087339.
46. Seethalekshmi, S.; Row, T.N.G. Conformational Polymorphism in a Non-Steroidal Anti-Inflammatory Drug, Mefenamic Acid. *Cryst. Growth Des.* **2012**, *12*, 4283–4289. https://doi.org/10.1021/cg300812v.
47. Lee, E.H.; Byrn, S.R.; Pinal, R. The Solution Properties of Mefenamic Acid and a Closely Related Analogue Are Indistinguishable in Polar Solvents but Significantly Different in Nonpolar Environments. *J. Pharm. Sci.* **2012**, *101*, 4529–4539. https://doi.org/10.1002/jps.23316.
48. Lozano, J.J.; Pouplana, R.; López, M.; Ruiz, J. Conformational Analysis of the Antiinflammatory Fenamates: A Molecular Mechanics and Semiempirical Molecular Orbital Study. *J. Mol. Struct. THEOCHEM* **1995**, *335*, 215–227. https://doi.org/10.1016/0166-1280(94)04003-B.
49. Ángel Nieto, I. Cristaloquímica de Cocristales de Aspirina Con Otros Fármacos Comunes. Master's Thesis, Benemérita Universidad Autónoma de Puebla, Puebla, Mexico, 2021.
50. Cesur, S.; Gokbel, S. Crystallization of Mefenamic Acid and Polymorphs. *Cryst. Res. Technol.* **2008**, *43*, 720–728. https://doi.org/10.1002/crat.200711119.
51. Cunha, V.R.R.; Izumi, C.M.S.; Petersen, P.A.D.; Magalhães, A.; Temperini, M.L.A.; Petrilli, H.M.; Constantino, V.R.L. Mefenamic Acid Anti-Inflammatory Drug: Probing Its Polymorphs by Vibrational (IR and Raman) and Solid-State NMR Spectroscopies. *J. Phys. Chem. B* **2014**, *118*, 4333–4344. https://doi.org/10.1021/jp500988k.
52. Lee, E.H.; Byrn, S.R.; Carvajal, M.T. Additive-Induced Metastable Single Crystal of Mefenamic Acid. *Pharm. Res.* **2006**, *23*, 2375–2380. https://doi.org/10.1007/s11095-006-9045-y.
53. Kons, A.; Mishnev, A.; Mukhametzyanov, T.A.; Buzyurov, A.V.; Lapuk, S.E.; Bē Rziņš, A. Hexamorphism of Dantrolene: Insight into the Crystal Structures, Stability, and Phase Transformations. *Cryst. Growth Des.* **2021**, *21*, 1190–1201. https://doi.org/10.1021/ACS.CGD.0C01508.
54. Polavarapu, P.L. Molecular Structure Determination Using Chiroptical Spectroscopy: Where We May Go Wrong? *Chirality* **2012**, *24*, 909–920. https://doi.org/10.1002/CHIR.22015.

55. Khodov, I.A.; Belov, K.V.; Pogonin, A.E.; Savenkova, M.A.; Gamov, G.A. Spatial Structure and Conformations of Hydrazones Derived from Pyridoxal 5′-Phosphate and 2-, 3-Pyridinecarbohydrazide in the Light of NMR Study and Quantum Chemical Calculations. *J. Mol. Liq.* **2021**, *342*, 117372. https://doi.org/10.1016/j.molliq.2021.117372.
56. Khodov, I.A.; Efimov, S.V.; Klochkov, V.V.; Batista De Carvalho, L.A.E.; Kiselev, M.G. The Importance of Suppressing Spin Diffusion Effects in the Accurate Determination of the Spatial Structure of a Flexible Molecule by Nuclear Overhauser Effect Spectroscopy. *J. Mol. Struct.* **2016**, *1106*, 373–381. https://doi.org/10.1016/j.molstruc.2015.10.055.
57. Khodov, I.A.; Nikiforov, M.Y.; Alper, G.A.; Blokhin, D.S.; Efimov, S.V.; Klochkov, V.V.; Georgi, N. Spatial Structure of Felodipine Dissolved in DMSO by 1D NOE and 2D NOESY NMR Spectroscopy. *J. Mol. Struct.* **2013**, *1035*, 358–362. https://doi.org/10.1016/j.molstruc.2012.11.040.
58. Tropp, J. Dipolar Relaxation and Nuclear Overhauser Effects in Nonrigid Molecules: The Effect of Fluctuating Internuclear Distances. *J. Chem. Phys.* **1979**, *72*, 6035–6043. https://doi.org/10.1063/1.439059.
59. Selivanov, S.I.; Shavva, A.G. An NMR Study of the Spatial Structure and Intramolecular Dynamics of Modified Analogues of Steroid Hormones. *Russ. J. Bioorganic Chem.* **2002**, *28*, 194–208. https://doi.org/10.1023/A:1015704203799.
60. Shavva, A.G.; Selivanov, S.I.; Starova, G.L.; Abusalimov, S.N. Synthesis and Investigation of the Spatial Arrangement of the 17β-Acetoxy-7α,18-Dimethyl-3-Methoxy-6-Oxaestra-1,3,5(10),8(9) -Tetraene. *Russ. J. Org. Chem.* **2006**, *42*, 198–205. https://doi.org/10.1134/S1070428002120072.
61. Woessner, D.E. Spin Relaxation Processes in a Two-Proton System Undergoing Anisotropic Reorientation. *J. Chem. Phys.* **1962**, *36*, 1–4. https://doi.org/10.1063/1.1732274.
62. Belov, K.V.; Eremeev, I.E.; Sobornova, V.V.; Klochkov, V.V.; Khodov, I.A. The Spatial Structure of Macroheterocyclic Compounds, as a Key Factor Affecting the Course of the Macrocyclization Reaction. *Macroheterocycles* **2020**, *13*, 44–54. https://doi.org/10.6060/mhc200388k.
63. Lee, W.; Krishna, N.R. Influence of Conformational Exchange on the 2D NOESY Spectra of Biomolecules Existing in Multiple Conformations. *J. Magn. Reson.* **1992**, *98*, 36–48. https://doi.org/10.1016/0022-2364(92)90107-I.
64. Belov, K.V.; Dyshin, A.A.; Kiselev, M.G.; Krestyaninov, M.A.; Sobornova, V.V.; Khodov, I.A. Determination of the Spatial Structure of Lidocaine in SC-CO2 by the 2D NOESY Method. *Russ. J. Phys. Chem. B* **2021**, *15*, 1303–1309. https://doi.org/10.1134/S1990793121080145.
65. Bame, J.; Hoeck, C.; Carrington, M.J.; Butts, C.P.; Jäger, C.M.; Croft, A.K. Improved NOE Fitting for Flexible Molecules Based on Molecular Mechanics Data-a Case Study with: S -Adenosylmethionine. *Phys. Chem. Chem. Phys.* **2018**, *20*, 7523–7531. https://doi.org/10.1039/c7cp07265a.
66. Gamov, G.A.; Khodov, I.A.; Belov, K.V.; Zavalishin, M.N.; Kiselev, A.N.; Usacheva, T.R.; Sharnin, V.A. Spatial Structure, Thermodynamics and Kinetics of Formation of Hydrazones Derived from Pyridoxal 5′-Phosphate and 2-Furoic, Thiophene-2-Carboxylic Hydrazides in Solution. *J. Mol. Liq.* **2019**, *283*, 825–833.
67. Jones, C.R.; Butts, C.P.; Harvey, J.N. Accuracy in Determining Interproton Distances Using Nuclear Overhauser Effect Data from a Flexible Molecule. *Beilstein J. Org. Chem.* **2011**, *7*, 145–150. https://doi.org/10.3762/bjoc.7.20.
68. Munro, S.L.A.; Craik, D.J. NMR Conformational Studies of Fenamate Non-Steroidal Anti-Inflammatory Drugs. *Magn. Reson. Chem.* **1994**, *32*, 335–342. https://doi.org/10.1002/MRC.1260320605.
69. Belov, K.V.; Dyshin, A.A.; Krestyaninov, M.A.; Efimov, S.V.; Khodov, I.A.; Kiselev, M.G. Conformational preferences of tolfenamic acid in DMSO-CO_2 solvent system by 2D NOESY. *J. Mol. Liq.* **2022**, *367*, 120481. https://doi.org/10.1016/j.molliq.2022.120481.
70. Khodov, I.A.; Belov, K.V.; Dyshin, A.A.; Krestyaninov, M.A.; Kiselev, M.G. Pressure effect on lidocaine conformational equilibria in scCO_2: A study by 2D NOESY. *J. Mol. Liq.* **2022**, *367*, 120525. https://doi.org/10.1016/j.molliq.2022.120525.
71. Khodov, I.A.; Musabirova, G.S.; Klochkov, V.V.; Karataeva, F.K.; Huster, D.; Holger, A.S. Structural details on the interaction of fenamates with lipid membranes. *J. Mol. Liq.* **2022**, *367*, 120502. https://doi.org/10.1016/j.molliq.2022.120502.